

Iron depletion strategy for targeted cancer therapy: utilizing the dual roles of neutrophil gelatinase-associated lipocalin protein

Hsin-Chieh Tang¹ · Pei-Chun Chang¹ · Yu-Chian Chen^{1,2,3}

Received: 10 August 2015 / Accepted: 21 December 2015
© Springer-Verlag Berlin Heidelberg 2016

Abstract Decreasing iron uptake and increasing iron efflux may result in cell death by oxidative inactivation of vital enzymes. Applying the dual function of neutrophil gelatinase-associated lipocalin (NGAL) could achieve the goal of iron depletion in the cancer cells. Tyr106, Lys125 or Lys134 was the key binding site for NGAL protein to sequester iron-chelating siderophores. In this study, we employed all bioactive peptides in peptide databank to dock with the siderophore-binding sites of NGAL protein by virtual screening. In addition, we performed molecular dynamics (MD) simulation to observe the molecular character and structural variation of ligand-protein interaction. Glu-Glu-Lys-Glu (EEKE), Glu-Glu-Asp-Cys-Lys (EEDCK), and Gly-Glu-Glu-Cys-Asp (GEECD) were selected preliminarily by rigorous scoring functions for further investigation. GEECD was excluded due to higher binding total energy than the others. Moreover, we also excluded EEKE due to larger influence to the stability of binding residues by the information of root mean square fluctuation (RMSF) and principal component analysis (PCA). Thus, we suggested that EEDCK was the potential bioactive peptide which had been proved to inhibit malignant cells for targeted cancer therapy.

Keywords Iron depletion · Molecular dynamics (MD) simulation · Neutrophil gelatinase-associated lipocalin (NGAL) · Peptide database · Principal component analysis (PCA) · Root mean square fluctuation (RMSF)

Introduction

Elemental iron is essential for many vital cellular functions, such as DNA synthesis that is basic for cell cycle progress, cell duplication, and growth. Iron is also implicated in free radical-generating reaction, reactive oxygen species, which produce a hydroxyl free radical which is deleterious to the cells. Damaged cells move toward either cell death or mutagenesis [1, 2]. Normal cells maintain fundamental iron level by the balanced regulation of transferrin (TF)-TF receptor, and ferroportin. Most cancer cells modify original cellular iron metabolism to meet the need of large amounts of iron [3]. Iron depletion strategy may result in cell death accompanied by oxidative inactivation of vital enzymes [4]. Cancer cells get net iron influx through increasing iron uptake by up-regulation of transferrin-TF receptors, and decreasing iron efflux by down-regulation of ferroportins [5, 6]. TF receptor antibody is the exploited therapeutic method to block iron uptake by these malignant cells [7]. However, these tricky malignant cells have another way to gain extra iron influx. Neutrophil gelatinase-associated lipocalin (NGAL, lipocalin 2, 24p3) is the magic tool of these cancer cells [8].

The well-known function of NGAL is about its innate immunity to limit bacteria growth through sequestering iron-chelating siderophore which is necessary for bacterial iron-dependant DNA synthesis. In human, NGAL transports iron into the cells and releases iron for certain DNA synthesis and enzyme expression. After sequestering iron-chelating siderophore by NGAL, it needs a receptor for

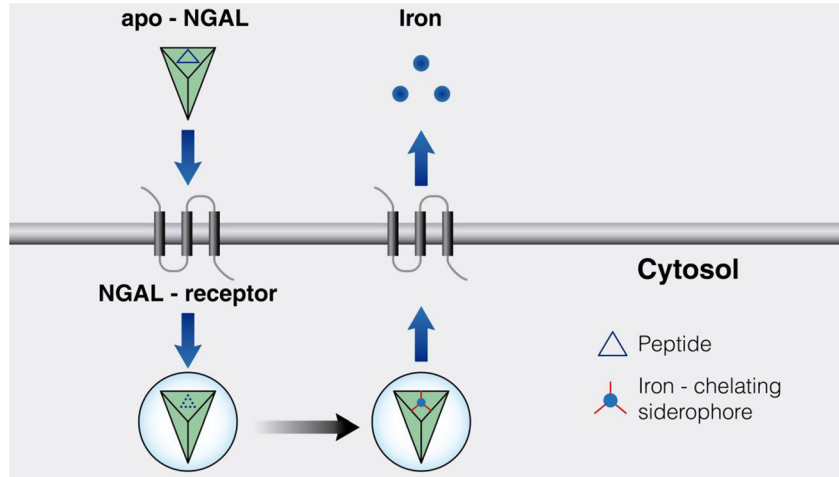
✉ Yu-Chian Chen
ycc929@mit.edu

¹ Department of Bioinformatics and Medical Engineering, Asia University, Taichung 41354, Taiwan

² Human Genetic Center, Department of Medical Research, China Medical University Hospital, Taichung 40402, Taiwan

³ Research Center for Chinese Medicine & Acupuncture, China Medical University, Taichung 40402, Taiwan

Scheme 1 Comprehension of the dual roles of neutrophil gelatinase-associated lipocalin protein

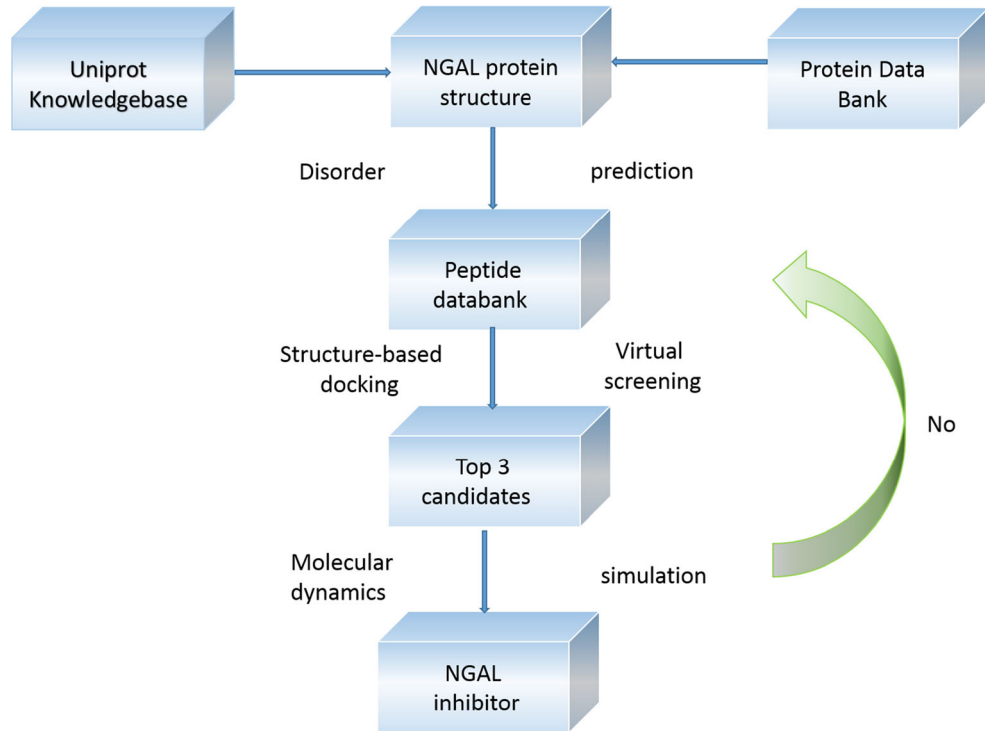


the NGAL-siderophore complex (holo-NGAL) to enter into the cell by endocytosis. In contrast, while empty NGAL without binding any siderophore (apo-NGAL) enters into the cell, it captures iron which is chelated by intracellular siderophore. Then the complex exits the cell membrane and decreases the iron level inside the cell. Iron depletion may lead to cell death finally [9–11]. According to the dual function of NGAL, it is the perfect target for cancer therapy. Occupying the siderophore-binding sites of NGAL outside the cell temporarily by a potential ligand until NGAL enters into the cell, and

releasing the siderophore-binding sites inside the cell might be a new resolution of iron depletion strategy for targeted cancer therapy (Scheme 1).

NGAL belongs to the lipocalin family which shares a similar backbone and is resistant to protease. They have a cylindrical or barrel shape, and a specific molecular binding site at the opening. The particular molecular binding sites are specific for their binding property. The human NGAL consists of the sequence of 198 amino acids. Residues 1–20 serve as the signal peptides, and residues 21–198 contribute to the main architecture. The key binding

Scheme 2 Overall screening and validation process



sites for sequestering iron-chelating siderophores are Tyr106, Lys125, and Lys134 [12, 13].

In this research, we attempted to apply the dual function of NGAL to achieve the goal of iron depletion in the cancer cells. Decreasing iron uptake in one hand and increasing iron efflux in the other hand were the main spirit of this research. We employed the peptide databank from Harvard University to search for the potential bioactive peptides that could bind to NGAL protein because the peptides would easily break down to constituent amino acids by the peptidase in the cytoplasm inside the cell. One could hardly find out the potential peptides from the large peptide databank by traditional one-by-one biochemistry [14]. The concept of computer-aided drug design might provide a feasible method to filter out the potential peptides efficiently [15, 16]. We carried out structure-based computational technique for preliminary selection. To select top candidates, molecular docking and virtual screening were initiated in prior to rigorous verification or validation [17]. The binding process for the docking stability of the candidates with NGAL could be verified or validated by molecular dynamics (MD) simulation (Scheme 2).

Materials and methods

Disordered sequence prediction

The sequence of human NGAL protein was acquired from the Uniprot Knowledgebase (P80188, 198 amino acids), and 3D crystal conformation of human NGAL protein was acquired from Protein Data Bank (PDB ID: 3U03). The ligand inside 3U03 was removed. For any compound or ligand to generate a subsequent influence on the function of the protein, interacting with the protein was an absolute requirement. The ideal structure or conformation of a protein had to be rigid. The more flexible the conformation of a protein was, the more difficult it was for the ligand to dock. Thus, prediction of the disordered sequence was necessary. We utilized the PONDR-FIT program in the DisProt website to predict the disordered sequence of the NGAL 3D structure. Above the value of 0.5 was the disordered sequence. In contrast, below the value of 0.5 was the rigid sequence.

Structure-based docking and virtual screening

We applied all the bioactive peptides from the peptide databank of Harvard University to dock with NGAL protein. There were 11,775 peptides in this peptide databank. Docking of a ligand with the target protein was a fundamental requirement to produce a ligand-protein interaction. It was essential to evaluate if a chosen or random

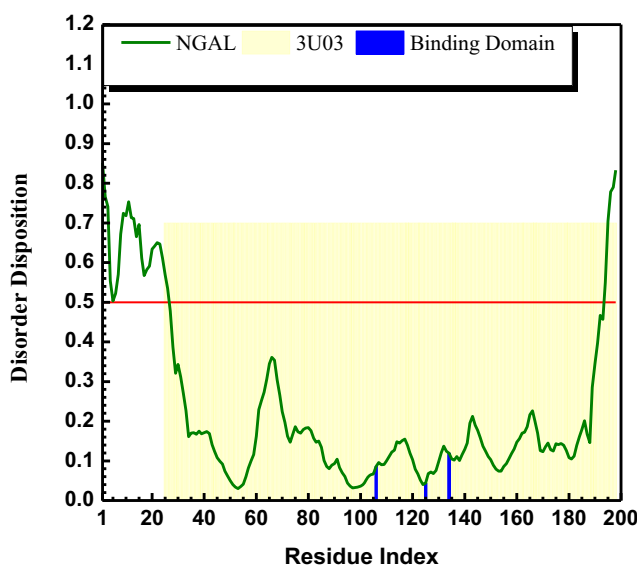


Fig. 1 Disordered sequence prediction. Above the value of 0.5 was the disordered sequence, and below the value of 0.5 was the rigid sequence in contrast

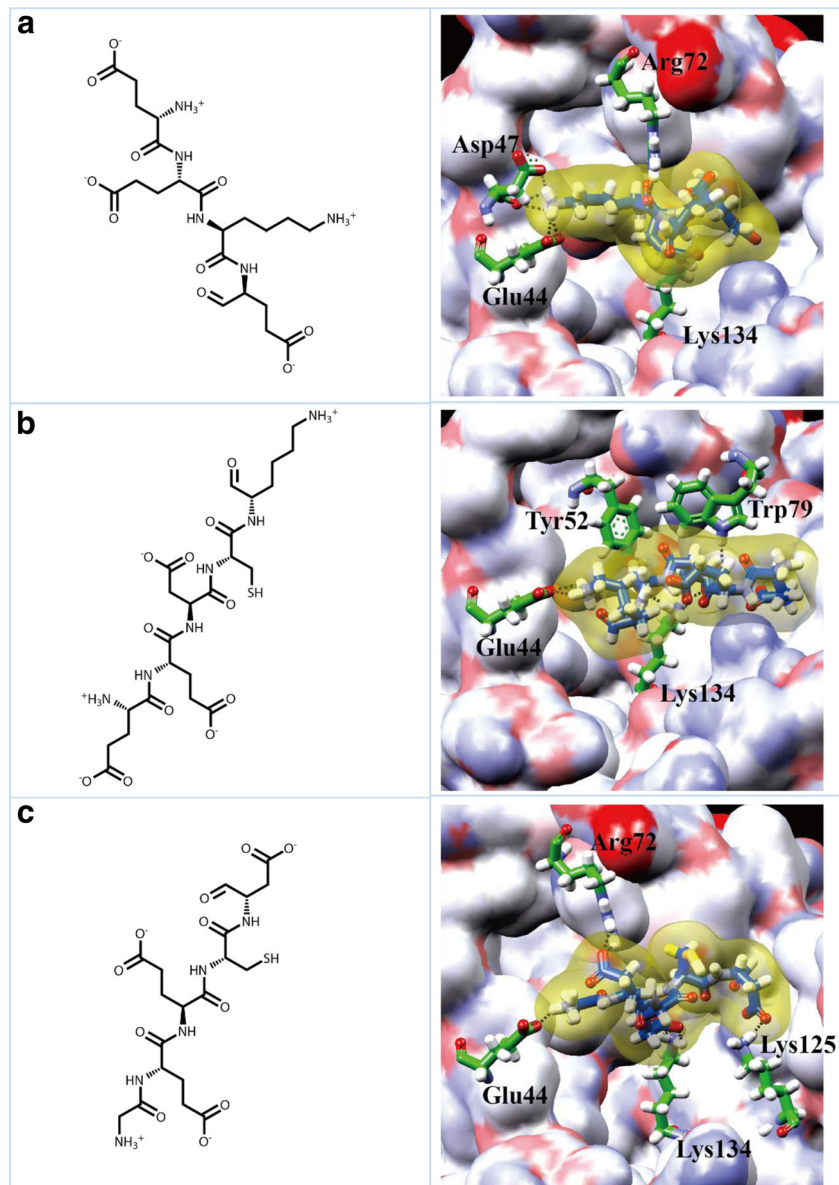
ligand could match the binding domain of the target NGAL protein. We minimized all of the docking poses between the ligands and NGAL protein by the force field method of Chemistry at HARvard Molecular mechanics (CHARMm). We applied LigandFit module in Accelrys Discovery Studio (DS) to perform docking procedure. The first course was to decide the binding sites of the NGAL protein. Main residues for the ligand's binding domain were set around the siderophore-bound sites. The second course was to yield the ligand's conformation

Table 1 Dock score of top ten bioactive peptides and siderophores

Name	Dock score	-PLP1	-PLP2
EEKE	393.243	44.91	50.27
EEDCK	385.355	41.22	51.22
GEECD	372.742	37.39	56.70
EEGSD	355.809	33.86	46.73
DGETC	344.873	33.07	47.00
EAESN	340.474	30.50	44.24
EAEHA	326.484	26.07	40.07
EPET	318.969	24.60	38.21
ADDK	311.140	23.88	35.90
KGEE	298.779	22.84	33.83
2_3-dihydroxybenzoic_acid ^a	97.221	18.43	32.19
2_5-dihydroxybenzoic_acid ^a	82.343	18.86	33.93
Catechol ^a	40.925	21.10	31.79

^a Siderophore

Fig. 2 Scaffold (left) and docking poses (right) of the peptides with NGAL protein by LigandFit. **a** EKEE. **b** EEDCK. **c** GEECD



by Monte Carlo method. Dock the ligand in the binding sites of NGAL protein. The third course was to estimate the binding affinity and scoring functions between the ligand and NGAL protein. LIGPROT program was

utilized to display the binding forces. We applied the scoring functions of Dock score, piecewise linear potentials 1 and 2 (-PLP1 and -PLP2) to compare the binding affinity for the ligands with NGAL protein [18, 19].

$$\text{Dock score} = -(\text{ligand internal energy} + \text{ligand/protein interaction energy}) \quad (1)$$

PLP1 indicated that except hydrogen atoms, each atom of the ligand and the protein was assigned a piecewise linear potential atom type. In addition to PLP1, an atomic radius was taken into consideration in PLP2 scoring function.

Molecular dynamics (MD) simulation

The binding or interaction of a ligand and NGAL protein was a dynamic process. It was necessary to analyze the enormous deviation or fluctuation data of the

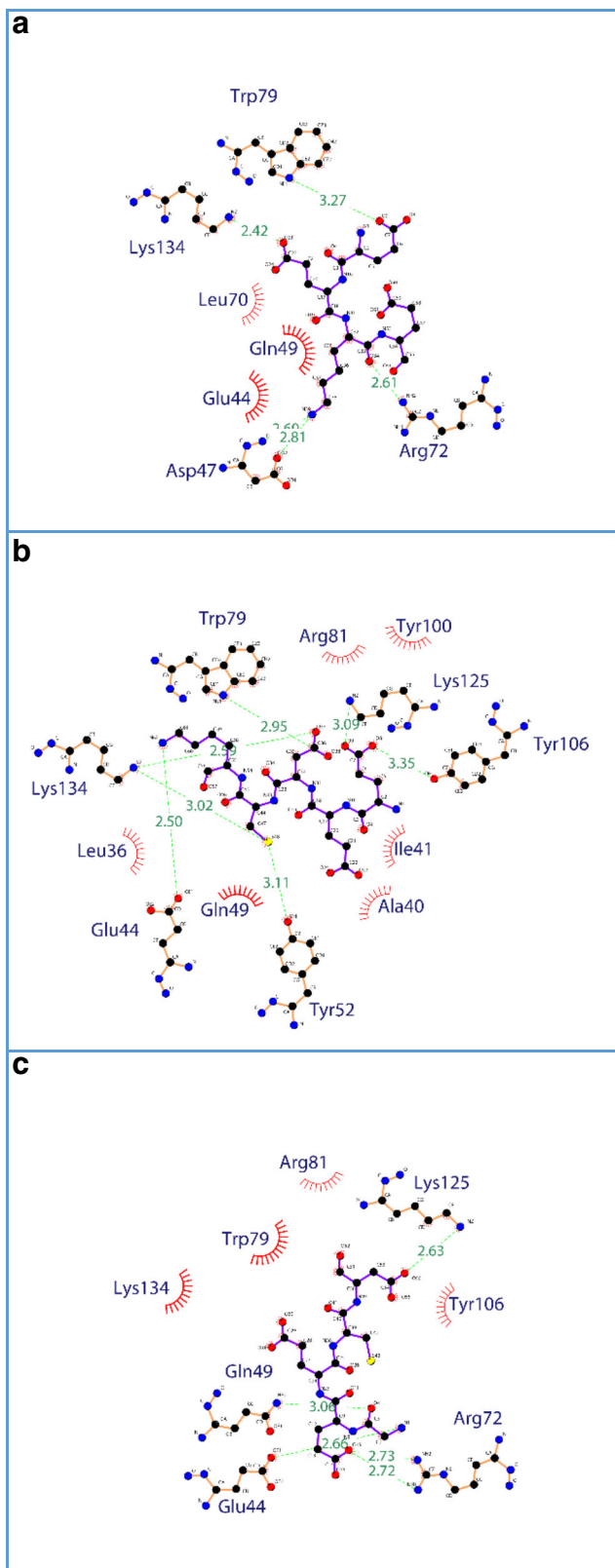


Table 2 H-bond occupancy of NGAL with EEKE peptide

H-bond interaction	Occupancy
HZ3:LYS134/O4:LIG179	10.19 %
HZ3:LYS134/O8:LIG179	43.56 %
HZ3:LYS134/O9:LIG179	60.54 %
HZ3:LYS134/O23:LIG179	75.72 %
HZ3:LYS134/O24:LIG179	56.74 %
HZ3:LYS134/O61:LIG179	20.68 %
HZ3:LYS125/O8:LIG179	76.92 %
HZ3:LYS125/O9:LIG179	10.99 %
HZ3:LYS125/O23:LIG179	15.98 %
HZ3:LYS125/O24:LIG179	41.66 %
HH:TYR106/O8:LIG179	70.23 %
HH:TYR106/O9:LIG179	92.61 %
HH22:ARG81/O9:LIG179	0.40 %
HH22:ARG81/O24:LIG179	24.28 %
HH12:ARG81/O24:LIG179	20.68 %
HE1:TRP79/O9:LIG179	1.70 %
HZ3:LYS73/O56:LIG179	4.80 %
HH22:ARG72/O4:LIG179	8.69 %
HH22:ARG72/O19:LIG179	10.19 %
HH22:ARG72/O34:LIG179	3.00 %
HH22:ARG72/O56:LIG179	1.40 %
HH22:ARG72/O60:LIG179	13.59 %
HH22:ARG72/O61:LIG179	5.79 %
HH12:ARG72/O4:LIG179	18.18 %
HH12:ARG72/O19:LIG179	22.98 %
HH12:ARG72/O34:LIG179	3.30 %
HH12:ARG72/O60:LIG179	20.98 %
HH12:ARG72/O61:LIG179	10.29 %
HE:ARG72/O56:LIG179	1.50 %
HG1:SER68/O24:LIG179	21.98 %
HH:TYR52/O23:LIG179	32.87 %
HH:TYR52/O24:LIG179	23.48 %
HE22:GLN49/O34:LIG179	0.60 %
HN:LEU42/O56:LIG179	4.30 %
OE1:GLU44/H52:LIG179	42.06 %
OE2:GLU44/H52:LIG179	48.35 %
OD1:ASP47/H52:LIG179	31.17 %
OD2:ASP47/H52:LIG179	24.38 %
O:ASP47/H52:LIG179	14.59 %
O:PRO48/H52:LIG179	3.80 %
OE1:GLN49/H52:LIG179	16.48 %
O:PHE71/H52:LIG179	4.80 %

Fig. 3 Docking poses of the peptides with NGAL protein by LIGPROT.

Table 3 H-bond occupancy of NGAL with EEDCK peptide

H-bond interaction	Occupancy
HZ3:LYS134/O9:LIG179	1.00 %
HZ3:LYS134/O37:LIG179	89.61 %
HZ3:LYS134/O38:LIG179	69.53 %
HE22:GLN128/O46:LIG179	0.30 %
HZ3:LYS125/O8:LIG179	0.70 %
HZ3:LYS125/O9:LIG179	99.90 %
HZ3:LYS125/O37:LIG179	3.10 %
HZ3:LYS125/O38:LIG179	96.20 %
HH:TYR106/O8:LIG179	99.60 %
HH:TYR106/O9:LIG179	93.61 %
HH22:ARG81/O8:LIG179	0.00 %
HH22:ARG81/O38:LIG179	0.80 %
HE:ARG81/O8:LIG179	1.40 %
HE1:TRP79/O8:LIG179	3.70 %
HE1:TRP79/O38:LIG179	1.30 %
HZ3:LYS73/O57:LIG179	1.00 %
HH22:ARG72/O23:LIG179	97.70 %
HH22:ARG72/O24:LIG179	98.30 %
HH12:ARG72/O23:LIG179	98.60 %
HH12:ARG72/O24:LIG179	99.30 %
HH:TYR52/O37:LIG179	1.30 %
HE22:GLN49/O57:LIG179	3.00 %
HN:LEU42/O57:LIG179	54.55 %
OH:TYR100/H77:LIG179	0.80 %
O:ALA40/H75:LIG179	2.80 %
O:LEU42/H75:LIG179	0.10 %
OE1:GLU44/H75:LIG179	30.87 %
OE2:GLU44/H75:LIG179	49.25 %
OD1:ASP47/H75:LIG179	1.90 %
OD2:ASP47/H75:LIG179	25.47 %
OE1:GLN128/H75:LIG179	1.40 %
OE1:GLN49/H63:LIG179	2.10 %

constituent atoms by MD simulation because a lot of atoms participated in the process of molecular interaction. It provided abundant information about the dynamic changes when a ligand bound to its target protein. We needed the mathematical algorithm to calculate and analyze the enormous dynamic data. The illustration of MD simulation was conducted by the GROningen MAchine for Chemical Simulations (GROMACS) program. Among the binding forces between the ligand and NGAL protein, hydrogen bond (H-bond) was the most important. We listed H-bond occupancy, and drew the H-bond distance trajectory of the ligands with NGAL protein. The existing distance of H-bond was less than 0.35 nm. The trajectories of root mean square deviation

Table 4 H-bond occupancy of NGAL with GEECD peptide

H-bond interaction	Occupancy
HZ3:LYS134/O30:LIG179	93.51 %
HZ3:LYS134/O31:LIG179	46.25 %
HZ3:LYS134/O41:LIG179	70.43 %
HZ3:LYS134/O55:LIG179	73.83 %
HZ3:LYS134/O56:LIG179	53.25 %
HZ3:LYS125/O55:LIG179	24.08 %
HZ3:LYS125/O56:LIG179	95.20 %
HH:TYR106/O55:LIG179	87.81 %
HH:TYR106/O56:LIG179	33.87 %
HH:TYR100/O52:LIG179	3.80 %
HH22:ARG81/O52:LIG179	5.29 %
HH22:ARG81/O55:LIG179	0.30 %
HE:ARG81/O52:LIG179	59.74 %
HE1:TRP79/O52:LIG179	27.37 %
HZ3:LYS73/O15:LIG179	4.40 %
HZ3:LYS73/O16:LIG179	4.70 %
HH22:ARG72/O15:LIG179	6.89 %
HH22:ARG72/O16:LIG179	7.69 %
HH12:ARG72/O15:LIG179	33.17 %
HH12:ARG72/O16:LIG179	41.56 %
HH:TYR52/O31:LIG179	99.30 %
HZ3:LYS50/O4:LIG179	5.29 %
HE22:GLN49/O4:LIG179	25.17 %
HE22:GLN49/N8:LIG179	29.37 %
HE22:GLN49/O11:LIG179	40.16 %
HE22:GLN49/N23:LIG179	31.37 %

(RMSD), radius of gyration, mean square displacement (MSD), total energy, and solvent accessible surface area (SASA) were drawn to evaluate molecular character of the ligand, protein, and complex. We illustrated root mean square fluctuation (RMSF), database of secondary structure assignment and component (DSSP), smallest distance matrices of residues, and principal component analysis (PCA) to evaluate structural variation of NGAL protein [20].

Results

Disordered sequence prediction

Main residues for the ligand's binding domain were set around the siderophore-bound sites, Tyr106, Lys125, and Lys134. They all fell in the rigid region below the value of 0.5 which indicated there was no influence on the shape of binding sites (Fig. 1).

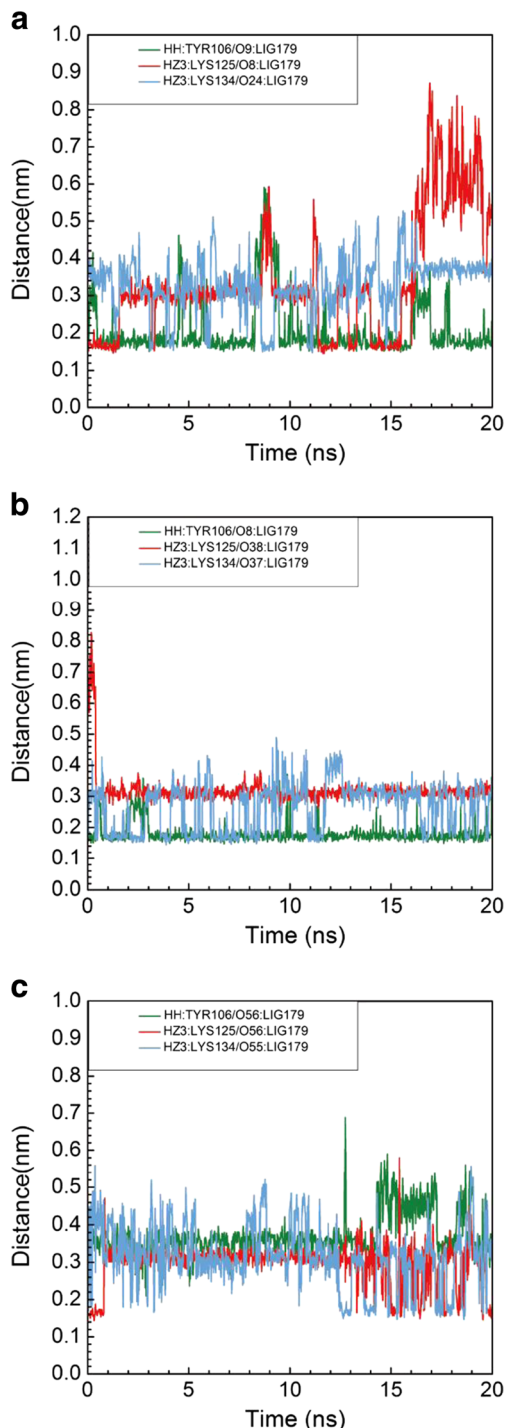


Fig. 4 The trajectories of distance for H-bonds. **a** EEKE. **b** EEDCK. **c** GEECD

Structure-based docking and virtual screening

We listed Dock score of the first ten peptides and representative siderophores (Table 1). The three peptides, Glu-Glu-Lys-Glu (EEKE), Glu-Glu-Asp-Cys-Lys (EEDCK), and Gly-Glu-Glu-Cys-Asp (GEECD) were

chosen as the top three candidates for further investigation. We displayed the binding forces between the three candidates and NGAL protein. EEKE formed hydrogen bonds (H-bonds) with Glu44, Asp47, Arg72, and Lys134 of NGAL protein. EEDCK formed H-bonds with Glu44, Tyr52, Trp79, and Lys134 of NGAL protein. GEECD formed H-bonds with Glu44, Arg72, Lys125, and Lys134 of NGAL protein (Fig. 2).

Glu44 and Lys134 were the common binding residues when the three candidates bound with NGAL protein. Lys134 was also one of the key binding sites for sequestering iron-chelating siderophore. Therefore, the three candidates had the opportunity to occupy the binding sites which were preserved for iron-chelating siderophore.

Besides H-bonds, hydrophobic contact was the other important binding force. EEKE formed hydrophobic contacts with Glu44, Gln47, and Leu70 of NGAL protein. EEDCK formed hydrophobic contacts with Leu36, Ala40, Ile41, Gln49, Arg81, and Tyr100 of NGAL protein. GEECD formed hydrophobic contacts with Trp79, Arg81, Tyr106, and Lys134 of NGAL protein (Fig. 3).

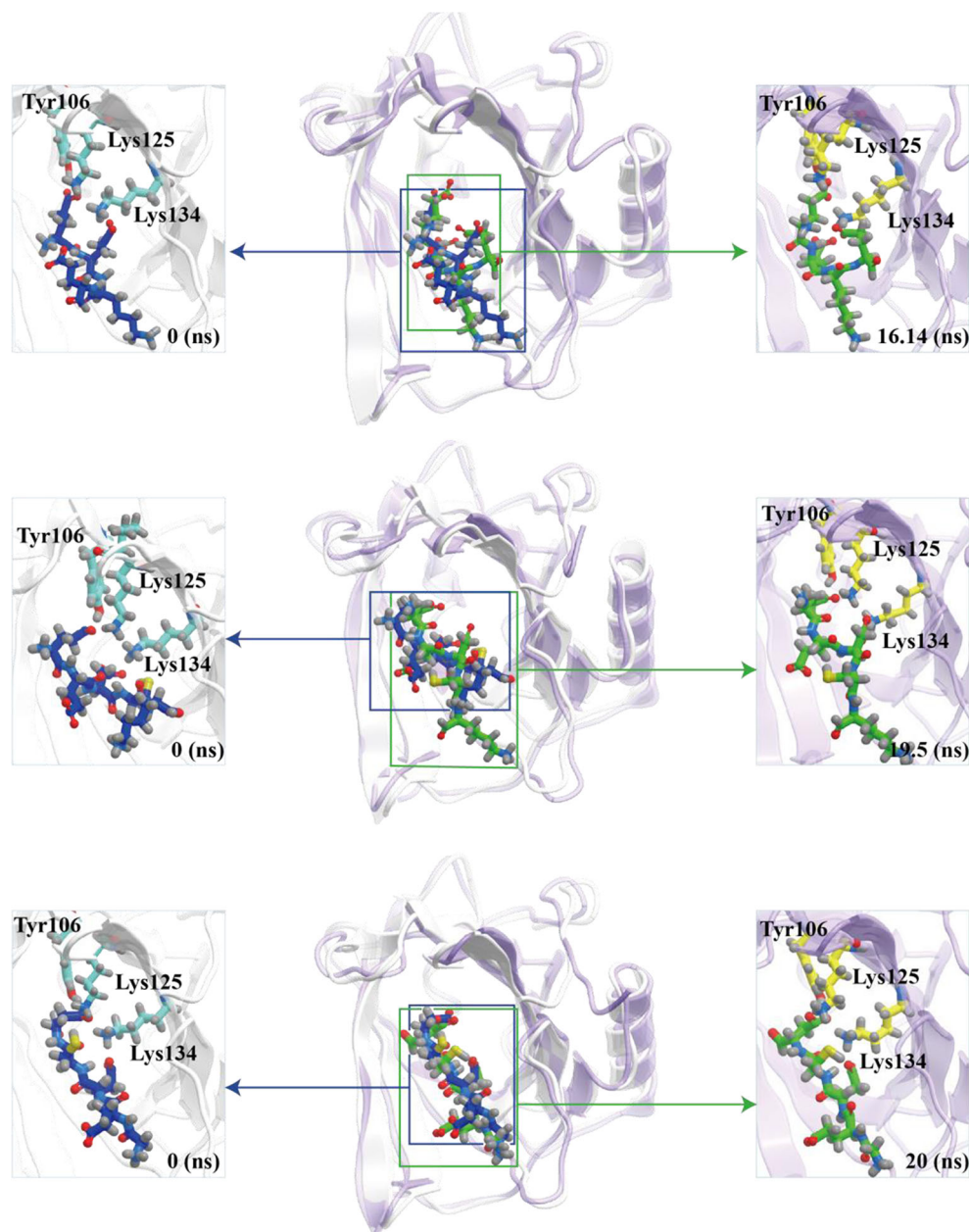
Molecular dynamics (MD) simulation

To survey the change of binding forces after molecular docking between the three candidates and NGAL protein, we illustrated the occupancy of H-bonds. The ratio number for occupancy of H-bonds indicated that total time ratio of the candidate could form H-bonds with specific residues of NGAL protein during MD period.

EEKE formed H-bond with Tyr106 of NGAL protein up to the ratio of 92.61 %, Lys125 up to 76.92 %, and Lys134 up to 75.72 % (Table 2). EEDCK formed H-bond with Tyr106 of NGAL protein up to the ration of 99.6 %, Lys125 up to 99.9 %, and Lys134 up to 89.61 % (Table 3). GEECD formed H-bond with Tyr106 of NGAL protein up to the ratio of 87.81 %, Lys125 up to 95.2 %, and Lys134 up to 93.51 % (Table 4).

The significant binding domains for sequestering iron-chelating siderophore of NGAL protein were Tyr106, Lys125, and Lys134. Although the three candidates did not occupy all the residues in the molecular docking, they did occupy Tyr106, Lys125, and Lys134 during MD period (Fig. 4). The three candidates bound to NGAL protein immediately accompanied with high affinity based on the Dock score. Soon after binding with NGAL protein, they changed their binding position to occupy the ligand-binding sites of NGAL around Tyr106, Lys125, and Lys134 which were the important binding residues for sequestering iron-chelating

Fig. 5 Binding position between the ligands and NGAL protein. EKEE (upper), EEDCK (middle). GEECD (lower)



siderophore. Thus, the three candidates could interfere with the binding of siderophore to NGAL protein (Fig. 5). This result might imply that decreasing iron uptake into the cancer cells would be possible by competitive inhibition of the three candidates.

In the following section, we displayed molecular character for the three candidates when they bound to NGAL protein. The trajectories of RMSD were illustrated to discuss the atoms' deviation during MD period. EKEE and EEDCK had larger average ligand 1 or ligand 2 deviation than GEECD. These results indicated that either EKEE and EEDCK had lower binding stability or

larger change of binding position. As previously described in the molecular docking, EKEE and EEDCK only occupied one of the key binding residues for siderophores (Lys134), but GEECD occupied two of the key binding residues (Lys125 and Lys134). The three candidates did occupy all the key binding residues (Tyr106, Lys125, and Lys134) during MD period. It demonstrated that the larger deviation of EKEE or EEDCK was due to larger change of binding position instead of lower binding stability.

Protein RMSD showed NGAL protein alone (apo) and the relevant NGAL protein of the three candidates

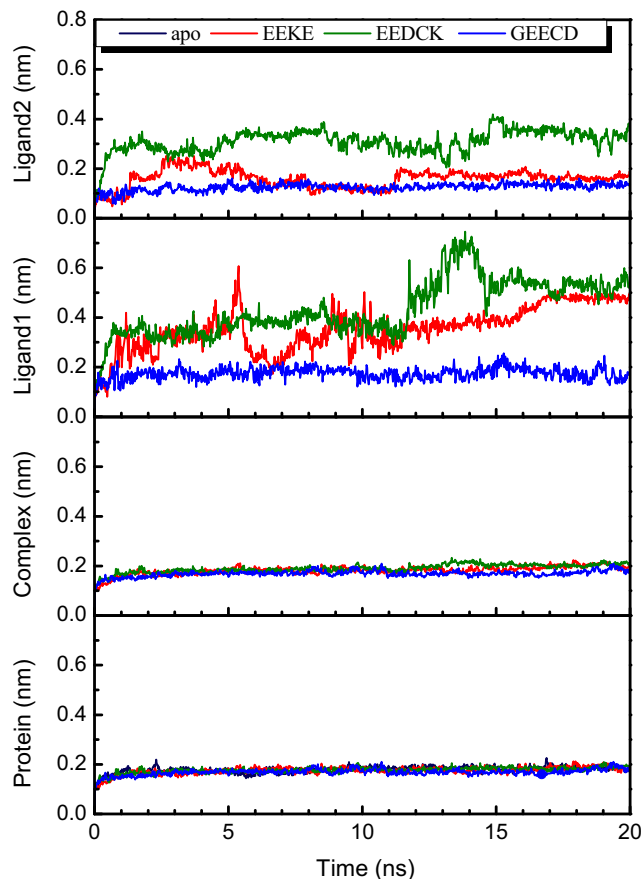


Fig. 6 The trajectories of root mean square deviation for ligand 2, ligand 1, complex, and protein RMSD

had almost the same average values. This result demonstrated that when the three candidates bound to NGAL protein, they nearly did not produce any conformational impact of NGAL protein. Complex RMSD displayed the sum of ligand and protein deviation (Fig. 6).

We illustrated the trajectories of gyrate to discuss the compact degree of the candidates and NGAL protein. Protein gyrate showed NGAL protein alone (apo) and the relevant NGAL protein of the three candidates had almost the same average values (Fig. 7A). Interestingly, the average ligand gyrate presented that EEDCK was larger than GEECD, and GEECD was larger than EKEE (Fig. 7b).

The trajectories of MSD were illustrated to discuss more detailed deviation of the candidates and NGAL protein. Average protein MSD showed that EKEE was higher than apo, but EEDCK and GEECD was lower than apo (Fig. 7c). Average ligand MSD presented that EEDCK was higher than EKEE, and EKEE was higher than GEECD (Fig. 7d).

To discuss binding stability when the three peptides bound with NGAL protein, we illustrated the frequency

of total energy. EKEE and EEDCK needed lower average energy to bind with NGAL protein, with which GEECD needed the highest average energy to bind. We suggested EKEE or EEDCK was able to bind with NGAL protein easier than GEECD (Fig. 7e). The trajectories of SASA were illustrated to discuss the water-contact surface area. Total SASA showed NGAL protein alone (apo) and the relevant NGAL protein of the three candidates had almost the same average values (Fig. 7f).

In the following section, we displayed structural variation of NGAL when the ligands bound. The histogram of RMSF was illustrated to discuss the fluctuation of the important binding amino acids, Tyr106, Lys125, and Lys134. Interestingly, EKEE relevant protein had higher RMSF value than NGAL protein alone (apo) in all of the important binding residues. This result means that EKEE produced larger impact to the conformation of binding domains. We could not estimate if there was any influence after EKEE released the important binding sites for the siderophores (Figs. 8 and 9). We performed DSSP to investigate the structural component changes of NGAL protein. Among these key binding residues, there were larger component changes around Lys125 (Fig. 10).

Smallest distance matrices of residues were illustrated to survey variation of the smallest distance for any two residues. There were no prominent differences between the relevant NGAL proteins for the candidates and apo (Fig. 11). We performed PCA to explore the identity of two eigenvectors according to the backbone of the candidate's relevant NGAL protein and apo. Among the eigenvectors of three candidates, EEDCK was almost consistent with NGAL protein alone (Fig. 12).

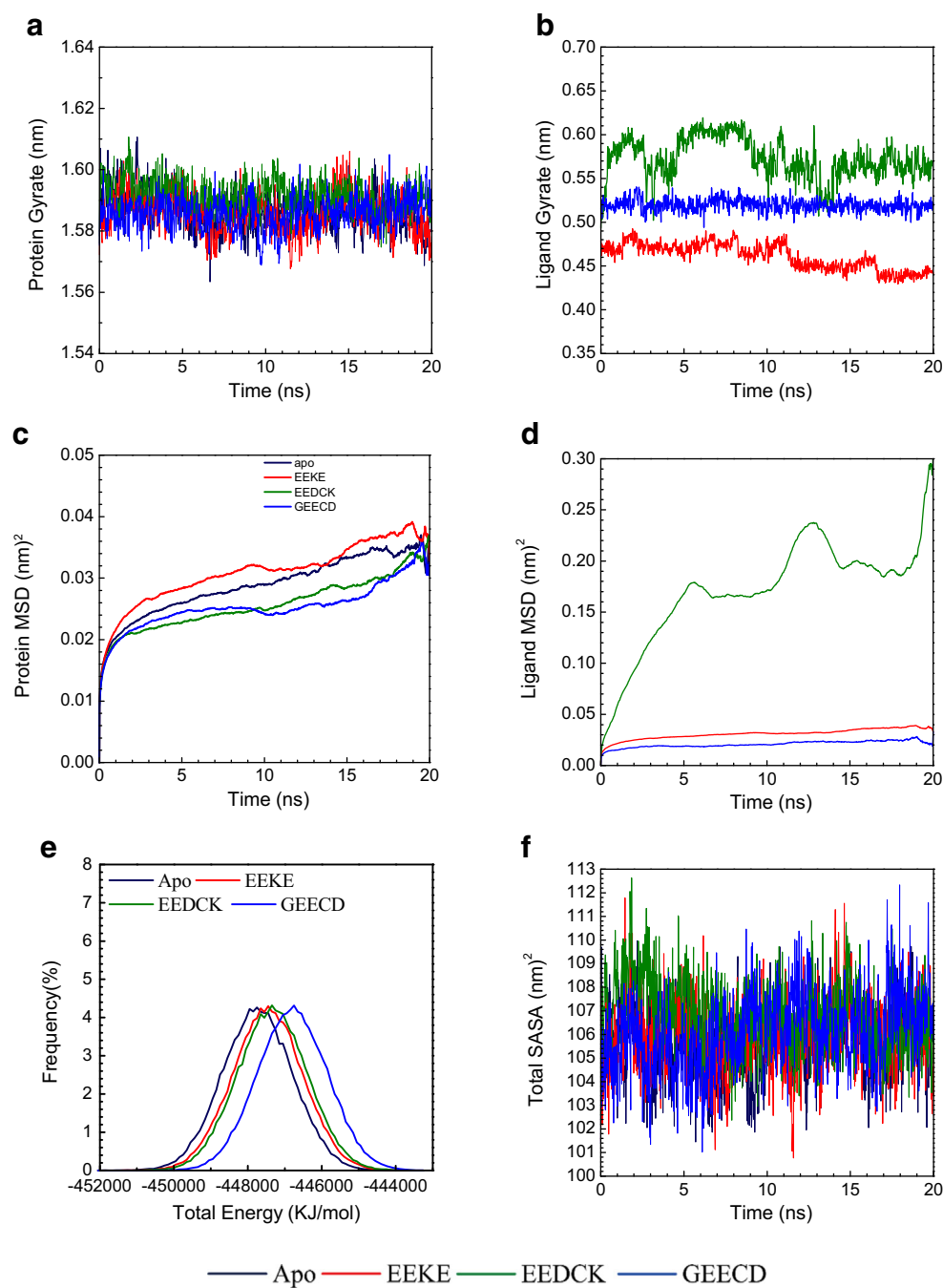
According to the MD simulation, we proposed that EEDCK to be the potential bioactive peptide for targeted cancer therapy.

Discussion

The critical situation for cancer disease is failure of cell growth control. Malignant cells accelerate proliferation rate and escape from apoptotic process. Therefore, cancer cells desire to obtain more and more materials needed for cell growth and replication. The materials contain all kinds of nutrient sources, such as glucose, fatty acids, amino acids, and ions [21–23].

Drug resistance is one of the major problems to traditional cancer therapy. The malignant cells develop many mechanisms that help these transformed cells flee from chemotherapy or other anticancer medicine. The drug resistant mechanisms contain drug inactivation, alternation of drug target,

Fig. 7 Molecular character for NGAL protein and the ligands when they produce protein-ligand interaction. **a** Protein gyrate. **b** Ligand gyrate. **c** Protein mean square displacement (MSD). **d** Ligand MSD. **e** Total energy. **f** Total solvent accessible surface area (SASA)



enhancing drug efflux, and running away from autophagy or apoptotic pathway [24–26].

Besides limiting bacteria growth, the significance of NGAL is related to acute kidney injury. Its blood and urine level is a prognostic indicator to access the severity of injury. It is believed that NGAL exhausts to rescue the cell [27]. Classic anti-acne medicine, isotretinoin, has the effect to limit the bacterial growth and induce sebaceous gland apoptosis [28, 29]. The drug appears to increase the releasing of NGAL through

retinoic acid receptor and retinoid X receptor [30]. These clinical studies indicate the three main roles of NGAL: limits bacteria growth, promotes cell survival, or seems to be opponent, induces cell apoptosis.

Either holo-NGAL or apo-NGAL can recognize NGAL receptor and enter into the cell, but the consequent fate is entirely different [31]. Further survey is needed to investigate whether holo-NGAL and apo-NGAL have the same binding affinity or not, and how the cells distinguish what type of NGAL they need.

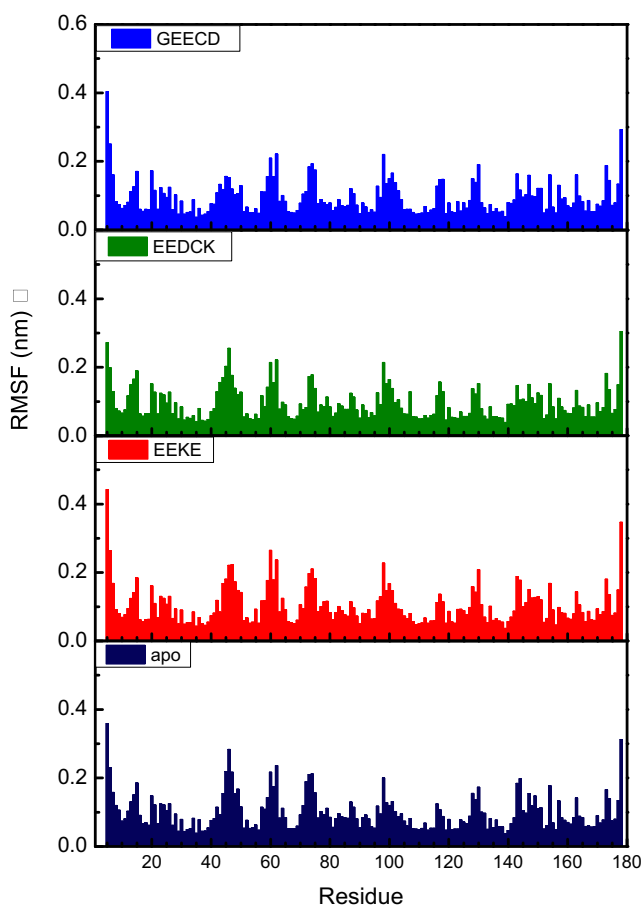


Fig. 8 The trajectories of root mean square fluctuation (RMSF)

Human NGAL receptor contains 538 amino acids, and does not have a clear crystal structure yet. Once the crystal structure of NGAL receptor is resolved, we can explore the secret of how it works.

Our study was to design drugs that could bind to NGAL and occupy the binding sites of siderophore. To achieve the goal of occupying the binding sites outside the cell and releasing them inside the cell, we chose peptide data bank to screen out the potential peptides. Peptides have been widely applied in drug therapy for metabolic disorders or peptide receptor-related diseases [32]. Although peptide had the character of being easily hydrolyzed, it was just proper for our requirement. There is exuberant enzymatic activity inside the cancer cells to produce amino acids from hydrolyzing foreign proteins or peptides. The malignant cells utilize these amino acids to generate energy by catabolism or promote new protein synthesis [33, 34]. One literature advocated that internalized NGAL might also be hydrolyzed inside the cells. Nevertheless this debate, inhibiting NGAL alone could achieve the strategy of iron depletion sufficiently [35].

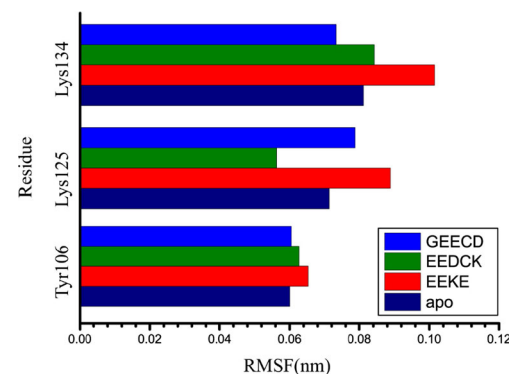


Fig. 9 The histogram of root mean square fluctuation for the relevant protein of three candidates and NAGL protein without any ligand (apo)

This research compared the binding affinity of three main biological siderophores when they bound to NGAL protein. 2, 3-dihydroxybenzoic acid was the main iron transporter of bacteria [36]. Catechol was the main iron-binding molecule in the circulation of human except transferrin [37]. 2, 5-dihydroxybenzoic acid was the main intracellular iron chelator of human cells [38]. Dock score of the listed ten peptides was higher than that of these biological siderophores. This result demonstrated that the three candidates could occupy the binding sites for extracellular siderophore, catechol, by competitive inhibition (Table 1).

The three peptide candidates could occupy the binding sites for sequestering iron-chelating siderophore of NGAL protein which conformation was not apparently changed by the ligand-protein interaction. Each binding site could bind one siderophore. Up to three siderophores could chelate one iron at the same time [13]. Therefore, if any one of the key binding sites was not occupied, the inhibitory effect would be discounted. All three candidates had the ability to occupy three key binding sites simultaneously. Thus, they would offer the best efficacy to interfere with the binding of siderophores (Tables 2, 3, and 4).

Conclusions

In this research, we proposed EEDCK to be the potential bioactive peptide for targeted cancer therapy. Previous study had demonstrated that pentapeptide EEDCK had an inhibitory effect on malignant cells due to the redox-mediated mechanism. Redox reaction was a reductive and oxidative reaction. Iron was implicated in redox cycling inside the cells. We provided prominent evidence to prove that EEDCK could bind to NGAL protein and might lead to iron depletion of cancer cells. This result would resolve the mechanism of how the pentapeptide EEDCK inhibited malignant cells [39, 40].

Fig. 10 Database of secondary structure assignment and component for (a) EEKE. b EEDCK. c GEECD. d apo

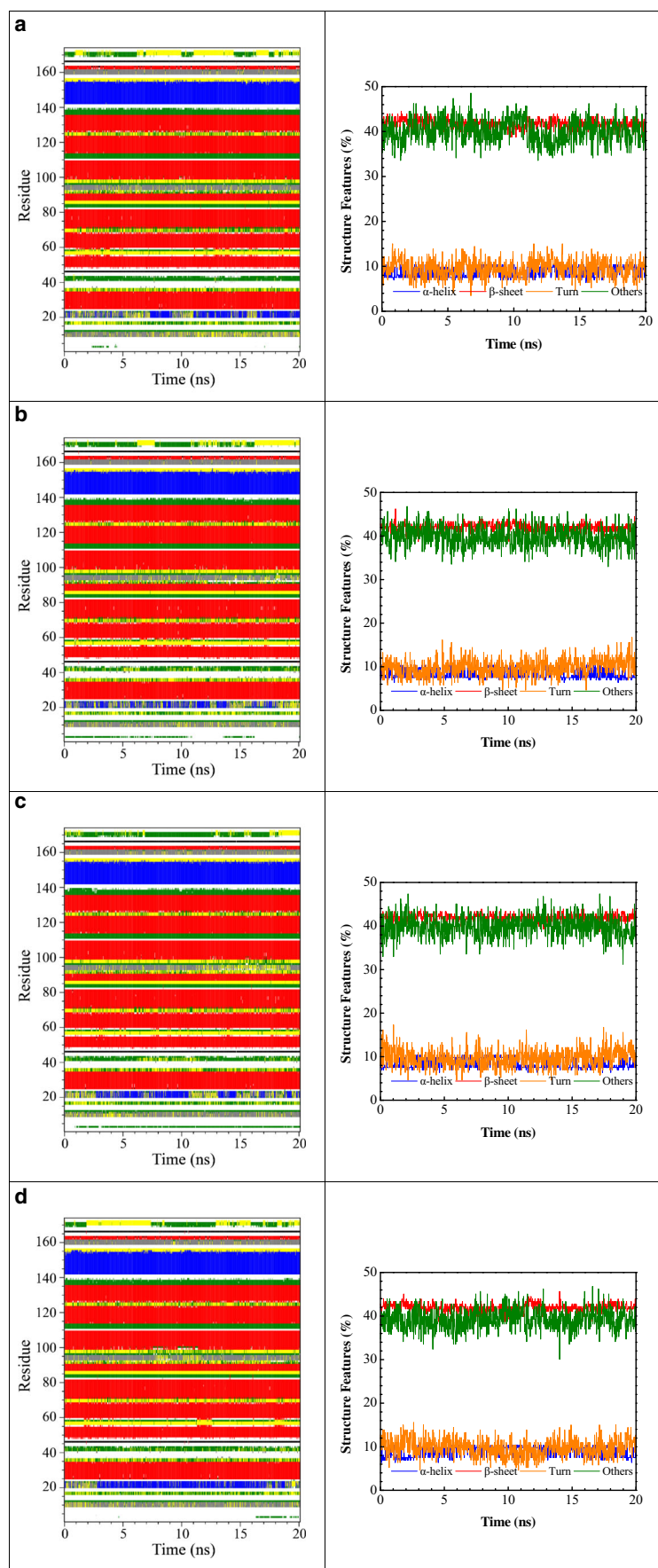


Fig. 11 Smallest distance matrices of residues for (a) EEKE, b EEDCK, c GEECD, d apo

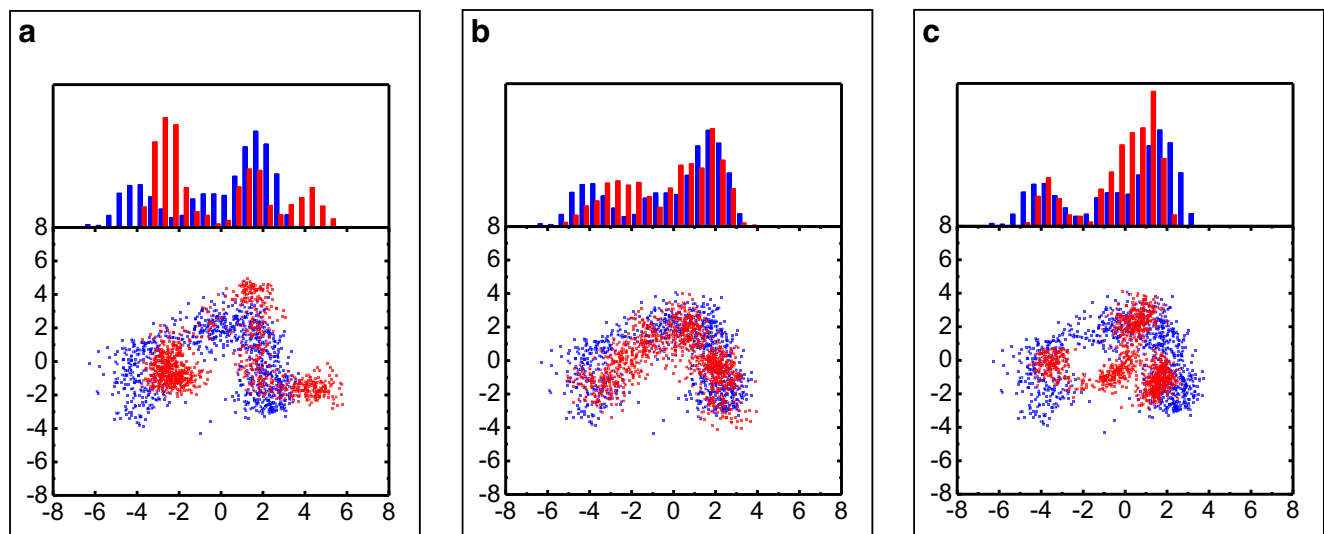
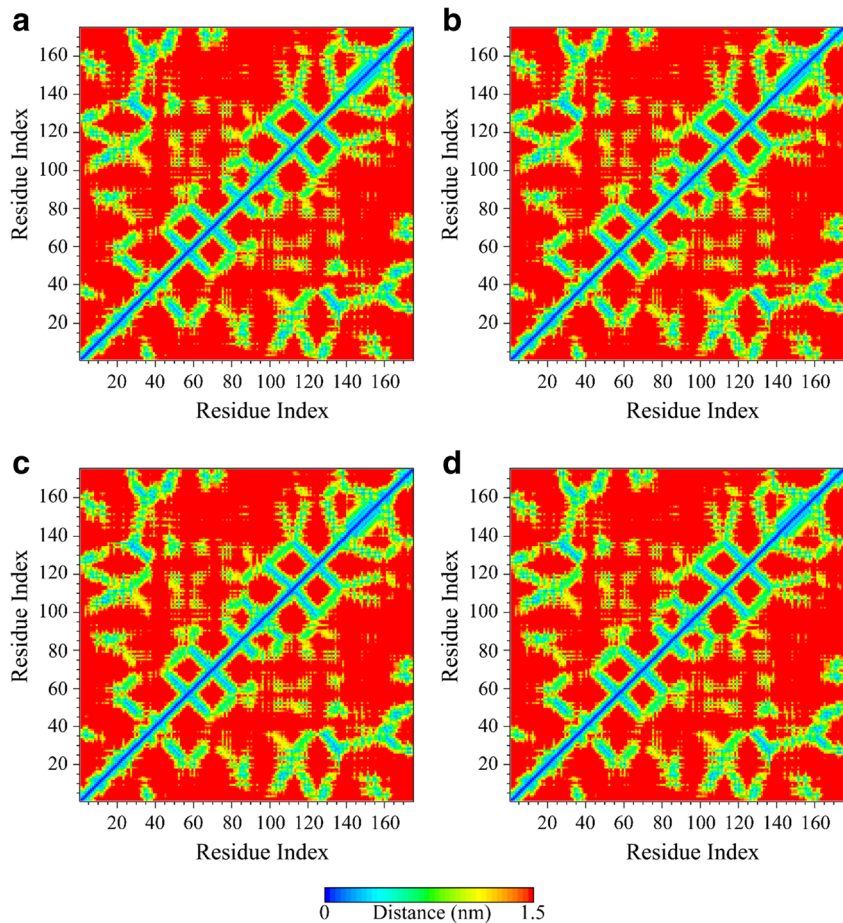


Fig. 12 Principal component analysis for (a) EEKE, (b) EEDCK, and (c) GEECD with NGAL protein alone (blue). Among the eigenvectors of three candidates (red), EEDCK was almost consistent with NGAL protein alone

Acknowledgments This research was supported by grants from Asia University (Asia102-CMU-1, Asia102-CMU-2, and Asia102-CMU-3), China Medical University Hospital (DMR-104-084, DMR-104-118, and DMR-102-001) and CMU under the Aim for Top University Plan of the Ministry of Education, Taiwan. This study was supported partly by the Taiwan Ministry of Health and Welfare Clinical Trial and Research Center of Excellence (MOHW105-TDU-B-212-113019).

References

- Schumacker PT (2015) Reactive oxygen species in cancer: a dance with the devil. *Cancer Cell* 27:156–157
- Bystrom LM, Guzman ML, Rivella S (2014) Iron and reactive oxygen species: friends or foes of cancer cells? *Antioxid Redox Signal* 20:1917–1924
- Torti SV, Torti FM (2013) Iron and cancer: more ore to be mined. *Nat Rev Cancer* 13:342–355
- Dixon SJ, Stockwell BR (2014) The role of iron and reactive oxygen species in cell death. *Nat Chem Biol* 10:9–17
- Andrews NC (2008) Forging a field: the golden age of iron biology. *Blood* 112:219–230
- Nagai K, Nakahata S, Shimosaki S, Tamura T, Kondo Y, Baba T, Taki T, Taniwaki M, Kurosawa G, Sudo Y, Okada S, Sakoda S, Morishita K (2014) Development of a complete human anti-human transferrin receptor C antibody as a novel marker of oral dysplasia and oral cancer. *Cancer Med* 3:1085–1099
- Daniels TR, Bernabeu E, Rodriguez JA, Patel S, Kozman M, Chiappetta DA, Holler E, Ljubimova JY, Helguera G, Penichet ML (2012) The transferrin receptor and the targeted delivery of therapeutic agents against cancer. *Biochim Biophys Acta* 1820:291–317
- Yang J, Goetz D, Li JY, Wang W, Mori K, Setlik D, Du T, Erdjument-Bromage H, Tempst P, Strong R, Barasch J (2002) An iron delivery pathway mediated by a lipocalin. *Mol Cell* 10:1045–1056
- Devireddy LR, Gazin C, Zhu X, Green MR (2005) A cell-surface receptor for lipocalin 24p3 selectively mediates apoptosis and iron uptake. *Cell* 123:1293–1305
- Schmidt-Ott KM, Mori K, Li JY, Kalandadze A, Cohen DJ, Devarajan P, Barasch J (2007) Dual action of neutrophil gelatinase-associated lipocalin. *J Am Soc Nephrol* 18:407–413
- Bolignano D, Donato V, Lacquaniti A, Fazio MR, Bono C, Coppolino G, Buemi M (2010) Neutrophil gelatinase-associated lipocalin (NGAL) in human neoplasias: a new protein enters the scene. *Cancer Lett* 288:10–16
- Correnti C, Richardson V, Sia AK, Bandaranayake AD, Ruiz M, Suryo Rahmanto Y, Kovacevic Z, Clifton MC, Holmes MA, Kaiser BK, Barasch J, Raymond KN, Richardson DR, Strong RK (2012) Siderocalin/Lcn2/NGAL/24p3 does not drive apoptosis through gentisic acid mediated iron withdrawal in hematopoietic cell lines. *PLoS One* 7, e43696
- Gomez-Casado C, Roth-Walter F, Jensen-Jarolim E, Diaz-Perales A, Pacios LF (2013) Modeling iron-catecholates binding to NGAL protein. *J Mol Graph Model* 45:111–121
- Tang HC, Chen YC (2015) Insight into molecular dynamics simulation of BRAF(V600E) and potent novel inhibitors for malignant melanoma. *Int J Nanomedicine* 10:3131–3146
- Mueller S, Coleman JR, Papamichail D, Ward CB, Nimnual A, Futcher B, Skiena S, Wimmer E (2010) Live attenuated influenza virus vaccines by computer-aided rational design. *Nat Biotechnol* 28:723–726
- Mandell DJ, Kortemme T (2009) Computer-aided design of functional protein interactions. *Nat Chem Biol* 5:797–807
- Tang HC, Chen YC (2015) Identification of tyrosinase inhibitors from traditional Chinese medicines for the management of hyperpigmentation. *Springerplus* 4:184
- Chen CY (2013) A novel integrated framework and improved methodology of computer-aided drug design. *Curr Top Med Chem* 13:965–988
- Vanommeslaeghe K, Hatcher E, Acharya C, Kundu S, Zhong S, Shim J, Darian E, Guvench O, Lopes P, Vorobyov I, Mackerell AD Jr (2010) CHARMM general force field: A force field for drug-like molecules compatible with the CHARMM all-atom additive biological force fields. *J Comput Chem* 31:671–690
- Pronk S, Pall S, Schulz R, Larsson P, Bjelkmar P, Apostolov R, Shirts MR, Smith JC, Kasson PM, van der Spoel D, Hess B, Lindahl E (2013) GROMACS 4.5: a high-throughput and highly parallel open source molecular simulation toolkit. *Bioinformatics* 29:845–854
- Parks SK, Chiche J, Pouyssegur J (2013) Disrupting proton dynamics and energy metabolism for cancer therapy. *Nat Rev Cancer* 13: 611–623
- Liu X, Madhankumar AB, Slagle-Webb B, Sheehan JM, Surguladze N, Connor JR (2011) Heavy chain ferritin siRNA delivered by cationic liposomes increases sensitivity of cancer cells to chemotherapeutic agents. *Cancer Res* 71:2240–2249
- Iannetti A, Pacifico F, Acquaviva R, Lavorgna A, Crescenzi E, Vascotto C, Tell G, Salzano AM, Scaloni A, Vuttariello E, Chiappetta G, Formisano S, Leonardi A (2008) The neutrophil gelatinase-associated lipocalin (NGAL), a NF- κ B-regulated gene, is a survival factor for thyroid neoplastic cells. *Proc Natl Acad Sci U S A* 105:14058–14063
- Housman G, Byler S, Heerboth S, Lapinska K, Longacre M, Snyder N, Sarkar S (2014) Drug resistance in cancer: an overview. *Cancers (Basel)* 6:1769–1792
- Nemeth E, Tuttle MS, Powelson J, Vaughn MB, Donovan A, Ward DM, Ganz T, Kaplan J (2004) Hepcidin regulates cellular iron efflux by binding to ferroportin and inducing its internalization. *Science* 306:2090–2093
- Candido S, Maestro R, Polesel J, Catania A, Maira F, Signorelli SS, McCubrey JA, Libra M (2014) Roles of neutrophil gelatinase-associated lipocalin (NGAL) in human cancer. *Oncotarget* 5: 1576–1594
- Paragas N, Qiu A, Zhang Q, Samstein B, Deng SX, Schmidt-Ott KM, Viltard M, Yu W, Forster CS, Gong G, Liu Y, Kulkarni R, Mori K, Kalandadze A, Ratner AJ, Devarajan P, Landry DW, D'Agati V, Lin CS, Barasch J (2011) The Ngal reporter mouse detects the response of the kidney to injury in real time. *Nat Med* 17:216–222
- Duman H, Topal IO, Kocaturk E and Duman MA (2015) Evaluation of anxiety, depression, and quality of life in patients with acne vulgaris, and quality of life in their families. *Dermatologica Sinica* doi:10.1016/j.dsi.2015.07.002
- Liu WH, Liu TC, Mong MC (2015) Antibacterial effects and action modes of asiatic acid. *Biomedicine (Taipei)* 5:16
- Nelson AM, Zhao W, Gilliland KL, Zaenglein AL, Liu W, Thiboutot DM (2008) Neutrophil gelatinase-associated lipocalin mediates 13-cis retinoic acid-induced apoptosis of human sebaceous gland cells. *J Clin Invest* 118:1468–1478
- Richardson DR (2005) 24p3 and its receptor: dawn of a new iron age? *Cell* 123:1175–1177
- Sun A, Fang J, Yan J (2013) Advance and development in research of bacterial drug-resistance signaling mechanism and multiple antigenic peptide-based vaccines. *Zhejiang Da Xue Xue Bao Yi Xue Ban* 42:125–130
- Ward PS, Thompson CB (2012) Metabolic reprogramming: a cancer hallmark even warburg did not anticipate. *Cancer Cell* 21:297–308
- Prajapati SC, Chauhan SS (2011) Dipeptidyl peptidase III: a multi-faceted oligopeptide N-end cutter. *FEBS J* 278:3256–3276

35. Hvidberg V, Jacobsen C, Strong RK, Cowland JB, Moestrup SK, Borregaard N (2005) The endocytic receptor megalin binds the iron transporting neutrophil-gelatinase-associated lipocalin with high affinity and mediates its cellular uptake. *FEBS Lett* 579:773–777
36. Abergel RJ, Clifton MC, Pizarro JC, Warner JA, Shuh DK, Strong RK, Raymond KN (2008) The siderocalin/enterobactin interaction: a link between mammalian immunity and bacterial iron transport. *J Am Chem Soc* 130:11524–11534
37. Bao G, Clifton M, Hoette TM, Mori K, Deng SX, Qiu A, Viltard M, Williams D, Paragas N, Leete T, Kulkarni R, Li X, Lee B, Kalandadze A, Ratner AJ, Pizarro JC, Schmidt-Ott KM, Landry DW, Raymond KN, Strong RK, Barasch J (2010) Iron traffics in circulation bound to a siderocalin (Ngal)-catechol complex. *Nat Chem Biol* 6:602–609
38. Correnti C, Strong RK (2012) Mammalian siderophores, siderophore-binding lipocalins, and the labile iron pool. *J Biol Chem* 287:13524–13531
39. Masse A, Ramirez LH, Bindoula G, Grillon C, Wdzieczak-Bakala J, Raddassi K, Deschamps de Paillette E, Mencia-Huerta JM, Koscielny S, Potier P, Sainteny F, Carde P (1998) The tetrapeptide acetyl-N-Ser-Asp-Lys-Pro (Goralatide) protects from doxorubicin-induced toxicity: improvement in mice survival and protection of bone marrow stem cells and progenitors. *Blood* 91:441–449
40. Terui Y, Tomizuka H, Mishima Y, Ikeda M, Kasahara T, Uwai M, Mori M, Itoh T, Tanaka M, Yamada M, Shimamura S, Ishizaka Y, Ozawa K, Hatake K (1999) NH₂-terminal pentapeptide of endothelial interleukin 8 is responsible for the induction of apoptosis in leukemic cells and has an antitumor effect in vivo. *Cancer Res* 59:5651–5655